Anisotropic lattice compression and pressure-induced electronic phase transitions in Sr_2IrO_4

K. Samanta,[1] R. Tartaglia,[1] U. F. Kaneko,[2] N. M. Souza-Neto,[2] and E. Granado[1]

[1] *"Gleb Wataghin" Institute of Physics, University of Campinas, UNICAMP, Campinas, São Paulo 13083-859, Brazil*

[2] *Brazilian Synchrotron Light Laboratory (LNLS), Brazilian Center for Research in Energy and Materials (CNPEM), Campinas, São Paulo 13083-970, Brazil*

(Received 29 August 2019; revised manuscript received 30 January 2020; accepted 31 January 2020; published 18 February 2020)

The crystal lattice of Sr_2IrO_4 is investigated with synchrotron x-ray powder diffraction under hydrostatic pressures up to $P = 43$ GPa and temperatures down to 20 K. The tetragonal unit cell is maintained over the whole investigated pressure range, within our resolution and sensitivity. The c-axis compressibility $\kappa_c(P,T) \equiv -(1/c)(dc/dP)$ presents an anomaly with pressure at $P_1 = 17$ GPa at fixed $T = 20$ K that is not observed at $T = 300$ K, whereas $\kappa_a(P,T)$ is nearly temperature independent and shows a linear behavior with P. The anomaly in $\kappa_c(P,T)$ is associated with the onset of long-range magnetic order, as evidenced by an analysis of the temperature dependence of the lattice parameters at fixed $P = 13.7 \pm 0.5$ GPa. At fixed $T = 20$ K, the tetragonal elongation $c/a(P,T)$ shows a gradual increment with pressure and a depletion above $P_2 = 30$ GPa that indicates an orbital transition and possibly marks the collapse of the $J_{\text{eff}} = 1/2$ spin-orbit-entangled state. Our results support pressure-induced phase transitions or crossovers between electronic ground states that are sensed, and therefore can be probed, by the crystal lattice at low temperatures in this prototype spin-orbit Mott insulator.

DOI: 10.1103/PhysRevB.101.075121

I. INTRODUCTION

The effect of strong spin-orbit coupling in the physical properties of solids is an active area of research in contemporary condensed matter physics [1–4]. The $5d$-transition metal oxides, in particular the Ruddlesden-Popper series of strontium iridates $Sr_{n+1}Ir_nO_{3n+1}$, are of interest due to the rare combination of strong spin-orbit interaction and electronic correlations that leads to a spin-orbit-entangled Mott insulating state ($J_{\text{eff}} = 1/2$) [5–10]. According to powder diffraction experiments, the layered crystal structure of Sr_2IrO_4 ($n = 1$) can be well described under a tetragonal space group $I4_1/acd$, featuring a rotation of the IrO_6 octahedra by $\sim 11^\circ$ along the c axis [11,12]. A significant Dzyaloshinskii-Moriya-type (DM) antisymmetric exchange interaction leads to a canted magnetic structure with a weak ferromagnetic moment of 0.06–0.14 μ_B/Ir below $T_N = 240$ K at ambient pressure [12–14]. The in-plane magnetic canting angle is nearly locked to the octahedral rotation [5,6,15,16]. On the other hand, the $J_{\text{eff}} = 1/2$ state may be unstable against a slight distortion of the IrO_6 octahedra due to possible competing orbital configurations [16,17]. Application of external pressure is expected to induce changes in the interatomic distances and angles, which could tune such competing electronic ground states. It is also generally expected that an external pressure should favor a metallic against a Mott insulating state, since the compressed lattice should increase the hybridization of the atomic wave functions thereby increasing the bandwidths. However, a metallic state is not achieved up to at least 55 GPa in Sr_2IrO_4, and the resistivity displays a U-shaped curve with pressure [8,18,19]. Our recent combined synchrotron x-ray powder diffraction (XPD) and phonon Raman scattering study under pressure at room temperature revealed a first-order structural phase transition at $\sim$55 GPa, and anomalous phonon and lattice behavior below 40 GPa that are indicative of electronic instabilities [20]. On the other hand, it is desirable to extend the detailed crystallographic investigation of this system under pressure to the low-temperature region of the phase diagram, so the relevance of the electronic/magnetic ground states to the crystal lattice can be probed. Here we report a detailed XPD study in Sr_2IrO_4 under hydrostatic pressures up to $P = 43$ GPa and down to $T = 20$ K. The long-range magnetic order is shown to produce an increment of the c-axis compressibility $\kappa_c(P,T) \equiv -(1/c)(dc/dP)$, as revealed both by the pressure dependence (at low temperature) and the temperature dependence (at $P = 13.7 \pm 0.5$ GPa) of the lattice parameters. Also, the c/a ratio shows a depletion consistent with an orbital transition above $P_2 = 30$ GPa. Our results demonstrate that pressure-induced changes in the electronic/magnetic ground state of Sr_2IrO_4 have a measurable impact in the crystal lattice at low temperatures, and, conversely, such lattice anomalies can be used to investigate the nature of the electronic/magnetic transitions in this compound and related materials.

II. EXPERIMENTAL DETAILS

The Sr_2IrO_4 powder sample was synthesized by a standard high-temperature solid-state reaction mechanism as described in Ref. [20]. Pressure-dependent XPD measurements at low temperatures were carried out at the x-ray diffraction and spectroscopy (XDS) beamline of the Brazilian Synchrotron Light Laboratory (LNLS) [21] with $\lambda = 0.61986$ Å calibrated with a LaB_6 standard sample. The focal spot size is 90×40 μm^2, obtained with a Rh cylindrical mirror, a LN_2-cooled double flat Si(111) crystal monochromator, a Rh toroidal focusing mirror, and a Kirkpatrick-Baez mirror. The

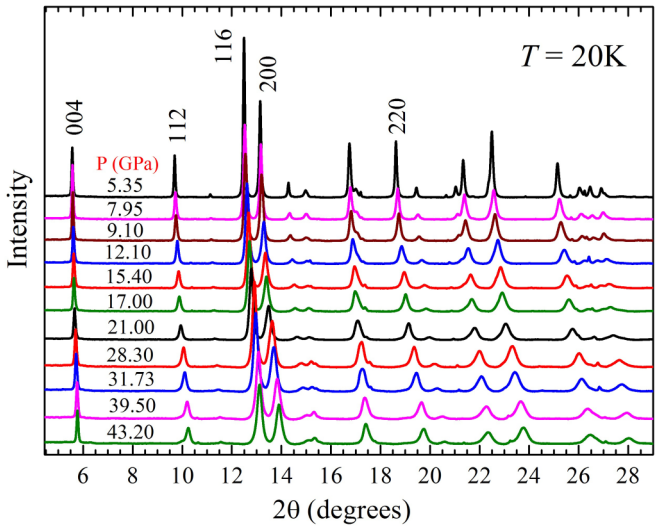

FIG. 1. Raw x-ray powder diffraction profiles for several pressures at $T = 20$ K ($\lambda = 0.61986$ Å). The Miller indices of selected reflections are indicated.

diffracted signal was detected in a transmission geometry by a 2D detector and the Debye ring intensities were integrated to yield conventional I versus 2θ diffractograms. A CuBe diamond anvil cell (DAC) was placed inside a continuous-flow liquid He cryostat. Boehler-Almax-type ultralow fluorescence diamonds with a cullet diameter of 350 μm were used to generate pressure. The pressure transmitting medium was helium, and gaskets were made of rhenium. The pressure values were obtained using the well-known ruby R_1 fluorescence line shift method. Pressure inside the DAC was controlled using a gas membrane. The pressure-dependent measurements were taken under increasing pressurization after the target temperature was stabilized. Temperature-dependent x-ray diffraction data at fixed pressure (13.7 ± 0.5 GPa) were collected under warming after cooling the cell with residual pressure (<5 GPa) and applying the desired pressure at the base temperature. The target pressure was checked at each temperature. For each measurement run (either pressure or temperature dependent), a new virgin sample was loaded into the pressure cell.

III. RESULTS AND ANALYSIS

Raw XPD profiles of Sr_2IrO_4 up to $P = 43$ GPa and at $T = 20$ K are shown in Fig. 1. Bragg peaks that are consistent with a tetragonal space group $I4_1/acd$ are observed in this pressure range, within our resolution and sensitivity. Rietveld refinements were performed to extract the lattice parameters of this phase under pressure. Since the accuracy of the Bragg intensities was limited by poor grain statistics (see Ref. [20]) and possible preferred orientation effects, the atomic positions and Debye-Waller factors were kept fixed in the refinements at the previously reported values for ambient pressure [12]. Figure 2 shows the fully observed and calculated diffraction

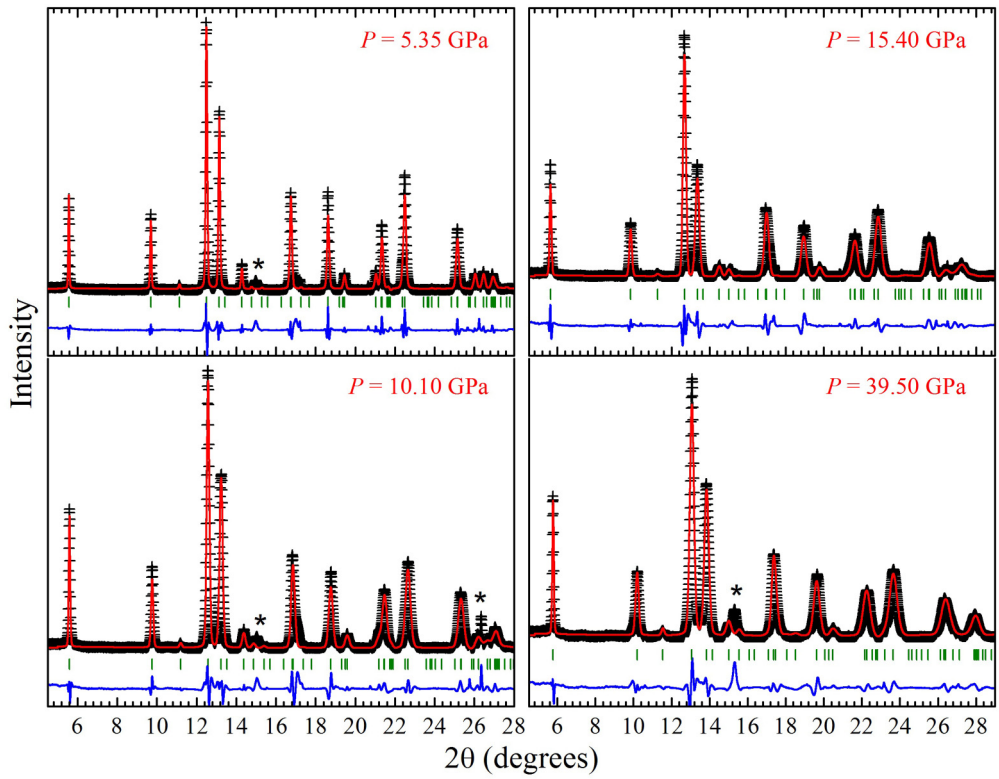

FIG. 2. Comparison between observed (open symbols) and calculated (red lines) x-ray powder diffraction profiles for selected pressures and $T = 20$ K. The differences are also shown (blue lines). The expected Bragg peak positions for the tetragonal $I4_1/acd$ space group are shown in short vertical bars. The spurious peaks identified by * are due to the rhenium gasket.

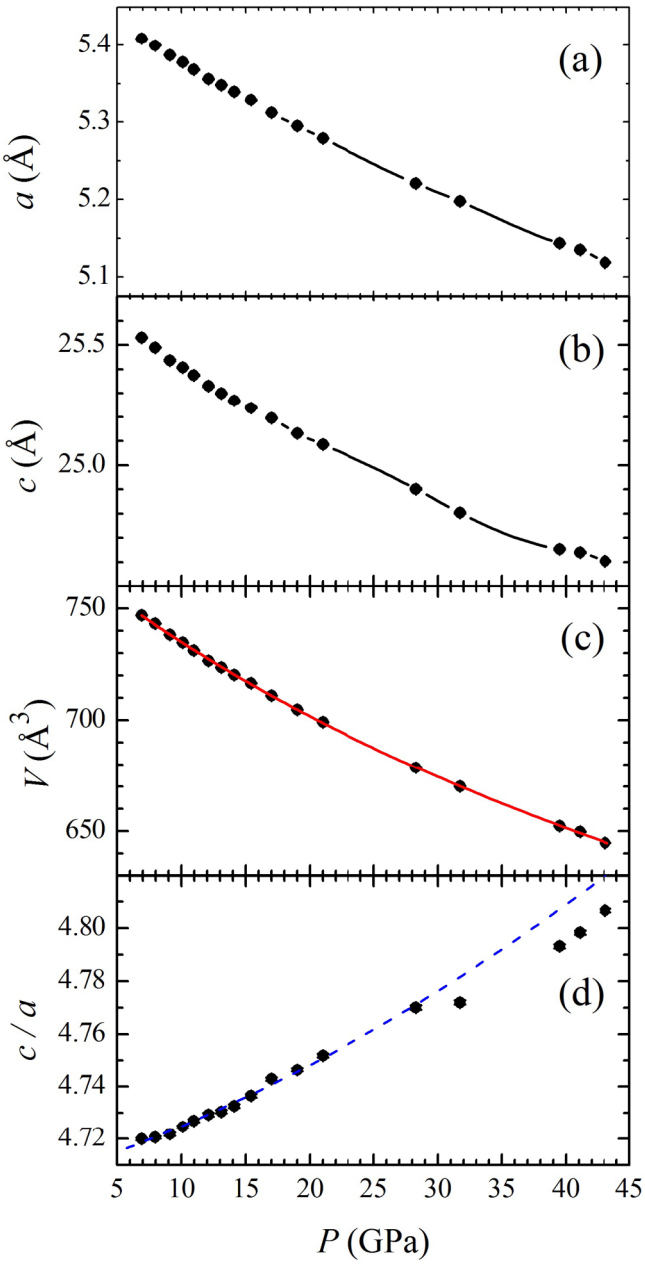

FIG. 3. Pressure dependence of the tetragonal lattice parameters a (a), c (b), unit cell volume V (c), and c/a ratio (d) at $T = 20$ K. The red solid line in (c) is a fitting according to the Murnaghan equation of state (see text). The blue dashed line in (d) is a second-order polynomial curve that captures the behavior below 30 GPa, and is shown as a guide to the eyes.

profiles at selected pressures, revealing sufficiently good fits that led to reliable refined lattice parameters.

The pressure dependence of the a and c lattice parameters at 20 K are shown in Figs. 3(a) and 3(b), respectively. The corresponding unit cell volume V is given in Fig. 3(c) (symbols). A Murnaghan equation of state [22], $P = (B_0/B_0')\{[V_0/V(P)]^{B_0'} - 1\}$, yielded a satisfactory fit [solid line in Fig. 3(c)], with the initial bulk modulus $B_0 = 162(3)$ GPa, initial bulk modulus derivative $B_0' = 3.6(2)$, and initial unit cell volume $V_0 = 777.0(8)$ Å^3. The tetragonal

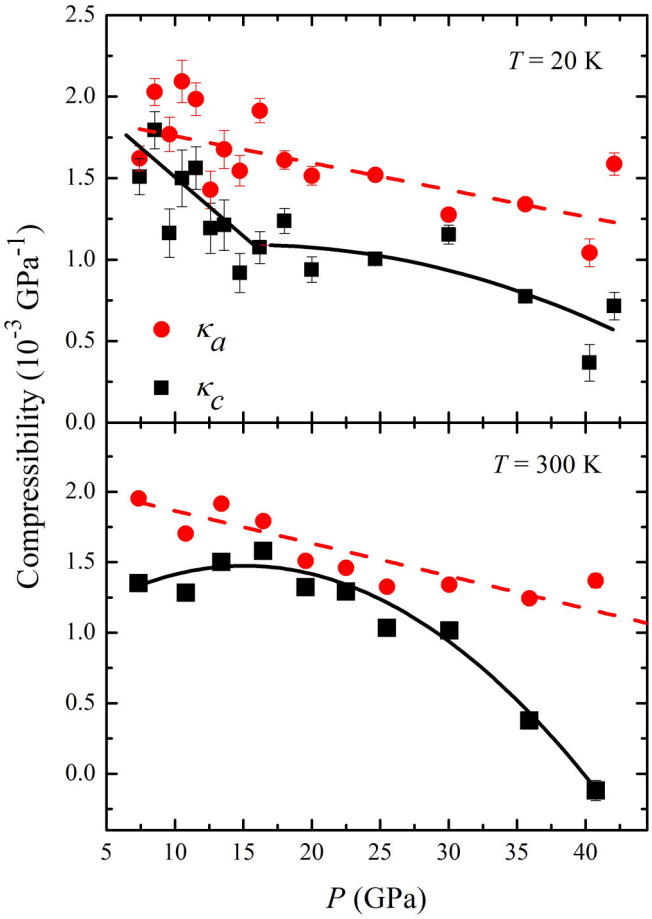

FIG. 4. Pressure dependence of the a-axis compressibility $\kappa_a \equiv -(1/a)(da/dP)$ and the c-axis compressibility $\kappa_c \equiv -(1/c)(dc/dP)$ at $T = 20$ K (a) and room temperature (b). The data in (b) were extracted from the results of Ref. [20]. The solid and dashed lines are guides to the eyes.

elongation (c/a ratio) is given in Fig. 3(d), increasing under pressurization. A clear anomaly in the c/a curve is seen at $P_2 \equiv 30$ GPa.

Figures 4(a) and 4(b) show the a- and c-axes compressibilities $\kappa_a(P)$ and $\kappa_c(P)$ obtained from the refined lattice parameters at 20 K (a) and room temperature (b), respectively, where the latter was extracted from the data shown in Ref. [20]. It can be seen that the $\kappa_a(P)$ curve is similar at both temperatures, showing a smooth reduction under increasing pressures, whereas $\kappa_c(P)$ is sensitive to temperature. In fact, at 20 K, $\kappa_c(P)$ decreases from $1.7(1) \times 10^{-3}$ GPa^{-1} at 7 GPa to $1.0(1) \times 10^{-3}$ GPa^{-1} at $P_1 \equiv 17$ GPa, remaining nearly constant at this value up to P_2 and further decreasing at higher pressures. At room temperature, $\kappa_c(P)$ remains nearly constant at $1.4(2) \times 10^{-3}$ GPa^{-1} between 7 GPa and P_1, then decreasing to $1.0(1) \times 10^{-3}$ GPa^{-1} at P_2 and steeply approaching zero at higher pressures.

In order to investigate whether the different $\kappa_c(P)$ curves at $T = 20$ K and $T = 300$ K may be related to a phase transition, more detailed temperature-dependent measurements are necessary. Since $\Delta c(P) = -\int_0^P \kappa_c(P')dP'$, the increased c-axis compressibility at low temperatures and low pressures

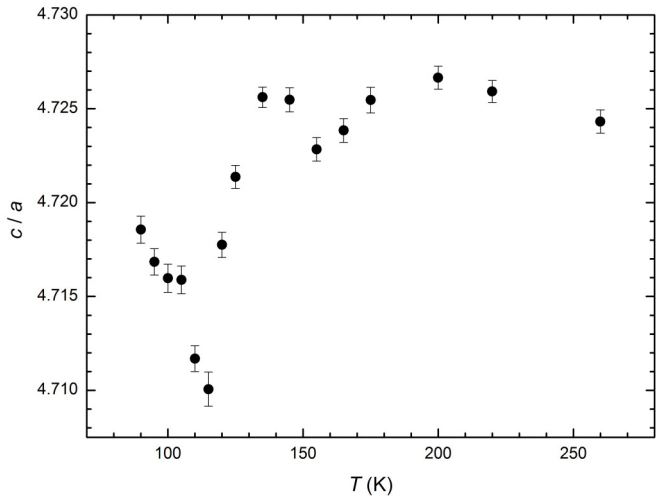

FIG. 5. Temperature dependence of the tetragonal elongation (c/a ratio) on warming under constant $P = 13.7 \pm 0.5$ GPa.

would be consistent with a larger integrated c-axis compression $-\Delta c(P)$ at 20 K with respect to room T in the low-pressure limit. In order to further investigate this effect, we obtained the temperature dependence of the lattice parameters on warming while keeping a nearly constant applied pressure 13.7 ± 0.5 GPa. Whereas the slight pressure variations for each change of temperature are sufficient to induce significant nonstatistical fluctuations for both a and c (not shown), the c/a ratio is much less sensitive to such pressure variations, yielding a physically meaningful temperature dependence (see Fig. 5). This ratio decreases steadily on warming up to ~115 K, shows a significant increment above this temperature, and finally stabilizes at a constant value $c/a = 4.725$ above 130 K. Considering that $\kappa_a(P)$ is temperature independent within our resolution, the increment of c/a ($P = 13.7$ GPa) above 115 K shown in Fig. 5 is consistent with the larger $\kappa_c(P)$ at low temperatures and low pressures with respect to room temperature and low pressures (see Fig. 4).

IV. DISCUSSION

The $\kappa_c(P)$ curves displayed in Figs. 4(a) and 4(b) indicate a change of behavior at $P_1 = 17$ GPa. Also, a clear anomaly in the c/a ratio is observed at $P_2 = 30$ GPa [see Fig. 3(d)]. Previous Raman scattering data at room temperature show significant phonon anomalies at both P_1 and P_2 [20]. Also, the magnetic XMCD signal and antiferromagnetic diffraction peaks at low temperatures disappear at P_1, whereas the XAS L_3/L_2 branching ratio appears to show a significant reduction above P_2 [18]. Taking all these independent data into consideration, there is compelling evidence of phase transitions or crossovers at these critical pressures, which are manifested at room temperature as well as at low temperatures. In short, the observed pressure-induced anomalies in the crystal lattice are likely related to modifications in the electronic structure of this material.

It can be seen in Figs. 3 and 4 that the lattice compression is anisotropic, consistent with previous data [18,20]. In fact, since $\kappa_a > \kappa_c$ for all pressures, the tetragonal elongation c/a increases with P [see Fig. 4(d)]. This is a reasonable trend, since the compression in the ab plane may occur both by a reduction of bond distances and by an increment of the tilt angle of the IrO_6 octahedra along the c axis, whereas only the first of these mechanisms is operative for the c-axis compression. Up to P_2, the increment of c/a ratio is well captured by a second-order polynomial [dashed line in Fig. 4(d)]. However, above P_2 the c/a ratio clearly falls below the extrapolated polynomial behavior. For pressures significantly above P_2, this ratio appears to re-establish the same increment rate as the extrapolated polynomial, however with a constant negative offset. This behavior is suggestive of an orbital transition at P_2 with an increment of Ir $5d$ electronic density in the ab plane above this pressure. Since the $5d$ electronic density in the ideal spin-orbit-entangled $J_{\text{eff}} = 1/2$ state shows cubic symmetry with equal xy, xz, and yz orbital occupations, the reported anomaly in the c/a ratio at P_2 is indicative of a breakdown of such a state. A possible scenario that is consistent with our data is a transition from a $J_{\text{eff}} = 1/2$ state at low pressures to a state with fully occupied xy orbitals and a hole in a combination of xz and yz orbitals above P_2. In fact, *ab initio* electronic calculations indicate that such state may be energetically viable with respect to the $J_{\text{eff}} = 1/2$ configuration [17].

The structural anomaly observed at P_1 appears to be more subtle with respect to that at P_2. In fact, no clear jump is observed in c/a, suggesting that Ir^{4+} orbital configuration is not substantially altered at P_1. This is consistent with the nearly constant L_3/L_2 XAS branching ratio through P_1 [18]. On the other hand, κ_c shows a clear change of behavior at P_1 and low temperatures [see Fig. 4(a)]. Our temperature-dependent lattice compression data at $P = 13.7$ GPa indicates that the increased compressibility at low pressures is related to a phase transition that occurs at $T^* \sim 115$–130 K (see Fig. 5), which coincides with T_N for this pressure (see Ref. [23]). It is therefore clear that the increment of κ_c at low pressures and low temperatures is associated with the presence of long-range magnetic order under these conditions. It is interesting to mention that the reduction of c/a below T^* at $P = 13.7$ GPa contrasts with the behavior at ambient pressure, where c/a increases below T_c [24]. Therefore, the anomalies in c/a shown in Fig. 5 most likely reflect the increment in κ_c in the magnetically ordered phase rather than a magnetoelastic coupling at zero pressure.

It is not very surprising that the lattice compressibility is sensitive to magnetic order. In fact, the magnetic energy may modify the lattice spring constants directly through the spin-phonon coupling [25–27], whereas less direct mechanisms involving the coupling of magnetic order to the electronic structure through the spin-orbit coupling might also affect the lattice stiffness. However, the sensitivity of κ_c but not κ_a to long-range magnetic order is interesting, considering that the exchange coupling in the ab plane is much stronger than along c. This result is likely a consequence of the much larger magnetic correlation length within the ab plane than along c in the paramagnetic phase of this material [28], which may effectively wash out the sensitivity of κ_a to the long-range magnetic ordering transition.

Finally, we should mention that anisotropic line shape broadenings of Bragg peaks were previously reported at room

temperature and for $P > P_1$ [20], which was interpreted as a possible sign of a symmetry-breaking instability. This line of reasoning led to the expectation that the crystal structure should suffer a long-range phase transition at P_1 for sufficiently low temperatures, which is however not confirmed by our present data at least at $T = 20$ K. An alternative explanation for the anisotropic line shape broadenings reported in Ref. [20] is based on the anisotropic compressibility of the crystal structure (see Fig. 4). Spatial fluctuations of the stress may occur and become more pronounced as the applied pressure increases. This may result in anisotropic strain fluctuations due to the different values of κ_a and κ_c, therefore leading to the anisotropic line shape broadenings of the Bragg peaks. On the other hand, it is interesting to note that for $Sr_3Ir_2O_7$, which is another member of this Ruddlesden-Popper series with $n = 2$, a tetragonal-monoclinic transition was observed at pressures close to 15 GPa [29], which is comparable to the critical pressure P_1 for Sr_2IrO_4. Further investigations are necessary to explore the similarities and differences between these related materials.

V. CONCLUSIONS

In summary, the lattice parameters of pressurized Sr_2IrO_4 show a tetragonal elongation that is increased significantly by hydrostatic pressures of the order of tens of GPa, with anomalies in κ_c at $P_1 = 17$ GPa at low temperatures and in the c/a ratio at $P_2 = 30$ GPa. The anomaly at P_2 is interpreted in terms of a transition between competing orbital configurations of the Ir $5d$ t_{2g} hole, whereas the anomaly of κ_c at P_1 is associated with the onset of long-range magnetic order.

ACKNOWLEDGMENTS

We thank D. Haskel and G. Fabbris for illuminating discussions and for sharing unpublished data, and M. Eleotério, J. Fonseca Júnior, and R. D. Reis for technical assistance. LNLS is acknowledged for concession of beamtime. This work was supported by Fapesp Grants 2016/00756-6, 2017/10581-1, and 2018/20142-8, and CNPq Grants 308607/2018-0 and 409504/2018-1, Brazil.

[1] C. L. Kane and E. J. Mele, Z_2 Topological Order and the Quantum Spin Hall Effect, Phys. Rev. Lett. **95**, 146802 (2005).

[2] B. A. Bernevig, T. L. Hughes, and S.-C. Zhang, Quantum spin Hall effect and topological phase transition in HgTe quantum wells, Science **314**, 1757 (2006).

[3] M. König, S. Wiedmann, C. Brüne, A. Roth, H. Buhmann, L. W. Molenkamp, X, -L. Qi, and S.-C. Zhang, Quantum spin Hall insulator state in HgTe quantum wells, Science **318**, 766 (2007).

[4] D. Pesin and L. Balents, Mott physics and band topology in materials with strong spin-orbit interaction, Nat. Phys. **6**, 376 (2010).

[5] B. J. Kim, H. Jin, S. J. Moon, J.-Y. Kim, B.-G. Park, C. S. Leem, J. Yu, T. W. Noh, C. Kim, S.-J. Oh, J.-H. Park, V. Durairaj, G. Cao, and E. Rotenberg, Novel $J_{\rm eff} = 1/2$ Mott State Induced by Relativistic Spin-Orbit Coupling in Sr_2IrO_4, Phys. Rev. Lett. **101**, 076402 (2008).

[6] B. J. Kim, H. Ohsumi, T. Komesu, S. Sakai, T. Morita, H. Takagi, and T. Arima, Phase-sensitive observation of a spin-orbital Mott state in Sr_2IrO_4, Science **323**, 1329 (2009).

[7] J. G. Rau, E. K.-H. Lee, and H.-Y. Kee, Spin-orbit physics giving rise to novel phases in correlated systems: Iridates and related materials, Annu. Rev. Condens. Matter Phys. **7**, 195 (2016).

[8] G. Cao and P. Schlottmann, The challenge of spin-orbit-tuned ground states in iridates: A key issues review, Rep. Prog. Phys. **81**, 042502 (2018).

[9] R. Arita, J. Kunes, A. V. Kozhevnikov, A. G. Eguiluz, and M. Imada, *Ab Initio* Studies on the Interplay between Spin-Orbit Interaction and Coulomb Correlation in Sr_2IrO_4 and Ba_2IrO_4, Phys. Rev. Lett. **108**, 086403 (2012).

[10] Q. Li, G. Cao, S. Okamoto, J. Yi, W. Lin, B. C. Sales, J. Yan, R. Arita, J. Kunes, A. V. Kozhevnikov, A. G. Eguiluz, M. Imada, Z. Gai, M. Pan, and D. G. Mandrus, Atomically resolved spectroscopic study of Sr_2IrO_4: Experiment and theory, Sci. Rep. **3**, 3073 (2013).

[11] Q. Huang, J. L. Soubeyroux, O. Chmaissem, I. Natali Sora, A. Santoro, R. J. Cava, J. J. Krajewski, and W. F. Peck, Jr., Neutron powder diffraction study of the crystal structures of Sr_2RuO_4 and Sr_2IrO_4 at room temperature and at 10 K, J. Solid State Chem. **112**, 355 (1994).

[12] M. K. Crawford, M. A. Subramanian, R. L. Harlow, J. A. Fernandez-Baca, Z. R. Wang, and D. C. Johnston, Structural and magnetic studies of Sr_2IrO_4, Phys. Rev. B **49**, 9198 (1994).

[13] S. Chikara, O. Korneta, W. P. Crummett, L. E. DeLong, P. Schlottmann, and G. Cao, Giant magnetoelectric effect in the $J_{\rm eff} = 1/2$ Mott insulator Sr_2IrO_4, Phys. Rev. B **80**, 140407(R) (2009).

[14] G. Cao, J. Bolivar, S. McCall, J. E. Crow, and R. P. Guertin, Weak ferromagnetism, metal-to-nonmetal transition, and negative differential resistivity in single-crystal Sr_2IrO_4, Phys. Rev. B **57**, R11039 (1998).

[15] F. Ye, S. Chi, B. C. Chakoumakos, J. A. Fernandez-Baca, T. Qi, and G. Cao, Magnetic and crystal structures of Sr_2IrO_4: A neutron diffraction study, Phys. Rev. B **87**, 140406(R) (2013).

[16] G. Jackeli and G. Khaliullin, Mott Insulators in the Strong Spin-Orbit Coupling Limit: From Heisenberg to a Quantum Compass and Kitaev Models, Phys. Rev. Lett. **102**, 017205 (2009).

[17] J. L. Lado and V. Pardo, Noncollinear versus collinear description of the Ir-based one-t_{2g}-hole perovskite-related compounds: $SrIrO_3$ and Sr_2IrO_4, Phys. Rev. B **92**, 155151 (2015).

[18] D. Haskel, G. Fabbris, M. Zhernenkov, P. P. Kong, C. Q. Jin, G. Cao, and M. van Veenendaal, Pressure Tuning of the Spin-Orbit Coupled Ground State in Sr_2IrO_4, Phys. Rev. Lett. **109**, 027204 (2012).

[19] D. A. Zocco, J. J. Hamlin, B. D. White, B. J. Kim, J. R. Jeffries, S. T. Weir, Y. K. Vohra, J. W. Allen, and M. B. Maple, Persistent non-metallic behavior in Sr_2IrO_4 and $Sr_3Ir_2O_7$ at high pressures, J. Phys.: Condens. Matter **26**, 255603 (2014).

[20] K. Samanta, F. M. Ardito, N. M. Souza-Neto, and E. Granado, First-order structural transition and pressure-induced lattice/phonon anomalies in Sr_2IrO_4, Phys. Rev. B **98**, 094101 (2018).

[21] F. A. Lima, M. E. Saleta, R. J. S. Pagliuca, M. A. Eleotério, R. D. Reis, J. Fonseca Júnior, B. Meyer, E. M. Bittar, N. M. Souza-Neto and E. Granado, XDS: A flexible Beamline for X-Ray Diffraction and Spectroscopy at the Brazilian Synchrotron, J. Synchrotron Radiat. **23**, 1538 (2016).

[22] F. D. Murnaghan, The compressibility of media under extreme pressures, Proc. Natl. Acad. Sci. **30**, 244 (1944).

[23] D. Haskel, G. Fabbris, J. H. Kim, L. S. I. Veiga, J. R. L. Mardegan, C. A. Escanhoela, Jr., S. Chikara, V. Struzhkin, T. Senthil, B. J. Kim, G. Cao, and J.-W. Kim, Possible Quantum Paramagnetism in Compressed Sr_2IrO_4, Phys. Rev. Lett. **124**, 067201 (2020).

[24] I. N. Bhatti, R. Rawat, A. Banerjee, and A. K. Pramanik, Temperature evolution of magnetic and transport behavior in 5*d* Mott insulator Sr_2IrO_4: Significance of magneto-structural coupling, J. Phys.: Condens. Matter **27**, 016005 (2014).

[25] W. Baltensperger and J. S. Helman, Influence of magnetic order in insulators on optical phonon frequency, Helv. Phys. Acta **41**, 668 (1968).

[26] E. Granado, A. García, J. A. Sanjurjo, C. Rettori, I. Torriani, F. Prado, R. D. Sanchez, A. Caneiro, and S. B. Oseroff, Magnetic ordering effects in the Raman spectra of $La_{1-x}Mn_{1-x}O_3$, Phys. Rev. B **60**, 11879 (1999).

[27] K. Samanta, D. Rigitano, P. G. Pagliuso, and E. Granado, Isospin-phonon coupling and Fano-interference in spin-orbit Mott insulator Sr_2IrO_4, Appl. Phys. Lett. **114**, 152402 (2019).

[28] S. Fujiyama, H. Ohsumi, T. Komesu, J. Matsuno, B. J. Kim, M. Takata, T. Arima, and H. Takagi, Two-Dimensional Heisenberg Behavior of $J_{\text{eff}} = 1/2$ Isospins in the Paramagnetic State of the Spin-Orbital Mott Insulator Sr_2IrO_4, Phys. Rev. Lett. **108**, 247212 (2012).

[29] J. Zhang, D. Yan, S. Yesudhas, H. Deng, H. Xiao, B. Chen, R. Sereika, X. Yin, C. Yi, Y. Shi, Z. Liu, E. M. Pärschke, C.-C. Chen, J. Chang, Y. Ding, and H.-k. Mao, Lattice frustration in spin-orbit Mott insulator $Sr_3Ir_2O_7$ at high pressure, npj Quantum Mater. **4**, 23 (2019).